Low-latency WDM intensity-modulation and direct-detection transmission over >100km distances in a hollow core fiber

Yang Hong, Kyle R. H. Bottrill, Thomas D. Bradley, Hesham Sakr, Gregory T. Jasion, Kerrianne Harrington, Francesco Poletti, Periklis Petropoulos, and David J. Richardson*

Dr. Yang Hong, Dr. Kyle R. H. Bottrill, Dr. Thomas D. Bradley, Dr. Hesham Sakr, Dr. Gregory T. Jasion, Dr. Kerrianne Harrington, Prof. Francesco Poletti, Prof. Periklis Petropoulos, and Prof. David J. Richardson
Optoelectronics Research Centre, University of Southampton,
Southampton SO17 1BJ, United Kingdom
*E-mail: y.hong@soton.ac.uk

Keywords: Hollow-core fibers, intensity-modulation and direct-detection, wavelength-division multiplexed transmission, low-latency communication

Our pervasive digital economy, fueled by developments in datacenter networking and cloud/edge computing, relies ever increasingly on the implementation of short- to metro-range high-capacity, low-latency optical communication links. In this paper, it is demonstrated that the low spectrally flat chromatic dispersion and ultralow nonlinearity possible in hollow-core fibers (HCFs) compared to conventional solid-core fibers offer significant potential for the transmission of intensity-modulation and direct-detection (IM-DD) signals over 100-km-scale distances. Specifically, the longest HCF-only IM-DD wavelength-division multiplexed (WDM) C-band transmission experiments (>100km) without chromatic dispersion compensation to date is reported, achieving reach improvements of approximately 5 times and 2 times compared to using standard single-mode fiber and non-zero dispersion-shifted fiber, respectively, in the same experimental recirculating loop set-up. For >100-km transmission, a significant >150-μs latency reduction can be obtained using HCF. These results, in combination with recent progress in loss reduction in HCFs, indicate that such fibers present a promising route to the realization of simple, cost-effective, high-capacity, ultra-low-latency IM-DD WDM transmission links with the potential to revolutionize optical networks in the years to come.

1. Introduction

The growth in significance of cloud/edge computing in recent years has placed particular emphasis on high-capacity optical links, the reach of which generally ranges from a few kilometres to around 100 kilometres, since moving the computation and data storage closer to the end user reduces response times and saves network bandwidth[1]-[2]. These systems already are, or will ultimately become, central to the implementation of various latency-sensitive real-time applications[3]. Some of these applications include intelligent transport systems, online financial trading, telemedicine, virtual reality streaming and high performance computing. An important consideration in cloud networking is latency, since it defines the geographical distribution of edge cloud infrastructure and hence the number of physical sites needed in cloud networks. In links longer than just a few kilometres, latency is dominated by the propagation time in the physical medium[4]-[6]. The signal propagation speed in conventional standard single-mode fibers (SSMFs) is essentially determined by the refractive index of the silica-based core-glass and only minimal improvements (in the region of 0.3%) can be achieved by adopting more complex refractive index profiles e.g. pure silica core designs[7]. Unlike conventional solid-core fibers, hollow-core fibers (HCFs) offer a fundamentally different route to realising light guidance as well as the potential to achieve lower fiber loss across the telecom bands (i.e. the O- to L-band)[8]-[10]. Light propagation at more than 99.8% of the light speed in vacuum can be achieved in HCFs, which thereby form the ultimate low-latency optical waveguide[8]. The approximately 50% increase in speed and hence ~33% reduction in latency that can be achieved by moving from solid silica fibers to HCFs provides increased network design flexibility for systems operating within a tightly constrained latency envelope and can potentially result in significant implementation benefits[8]. By confining the light signal in an air-guided core, HCFs also offer a significantly lower nonlinearity than conventional solid-core silica fibers[9] which provides the potential to overcome the nonlinear Shannon capacity limit of solid-core fibers[11]-[13]. Over the last few years, substantial progress has been reported in the development of

HCFs[14]-[17]. The lowest loss reported to date in an HCF is 0.28 dB/km in the telecom C and L bands, achieved in a nested antiresonant nodeless fiber (NANF)[17], opening up possibilities in the short-haul/metro application space. Should progress in fabrication continue at a similar pace, it may not be long before further loss reductions are possible, and HCFs can then be considered for long-haul applications as well, particularly in applications where latency is key. NANFs exhibiting an ultrawide optical transmission bandwidth have also been reported, for example offering low-loss, effectively single-mode guidance across wavelengths spanning from 1240-1940 nm (which covers the O- to L-band and beyond)[15], and there is the longer term potential to achieve lower losses in the O-band in NANFs relative to solid silica SMF[9]. Several transmission experiments have already explored the advantages of HCFs, demonstrating penalty-free[18], ultra-wideband[19] and mode-division multiplexed transmission[20]. These demonstrations have either used relatively short lengths of HCF (of the order 1-10 km) or have combined lengths of HCF and solid-core fibers in optical recirculating loops[21]-[22]. Even though the addition of solid-core transmission fibers in these latter demonstrations were generally used for purely practical reasons (i.e. to increase the loop transit time and to enable more reliable measurements), they have not allowed a full exploration of the benefits of the wideband, spectrally flat low dispersion profiles that HCF designs enable.

With particular reference to transmission in edge/cloud networks, it is also relevant to consider the simplicity and cost effectiveness of the implementation, since these factors largely dominate the associated hardware costs and network scalability. In this context, the adoption of simple intensity-modulation and direct-detection (IM-DD) transmission rather than coherent data transmission formats is appealing[23]. However, the reach and capacity of IM-DD transmission are severely restricted by the chromatic dispersion (CD) in SSMF due to the power fading it induces[23]-[24]. Although the O-band exhibits much lower CD in SSMF and lower cost lasers are available in this spectral region, the C-band is ultimately more desirable when considering extension of the transmission reach in IM-DD systems due to the lower fiber loss and the

availability of Erbium-doped fiber amplifiers (EDFAs). In IM-DD, CD can then be overcome/mitigated either by including dispersion compensating fibers in the transmission line (which adds an additional ~25% latency[5]), some other dispersion compensating device (e.g., a chirped fiber Bragg grating which adds additional loss and imposes bandwidth restrictions/complexity/cost), or by transmitting in dispersion-shifted fiber (DSF) instead, which can give rise to nonlinear system penalties. Another solution relies on the use of non-zero DSF (NZ-DSF), which moves the zero-dispersion wavelength outside of the conventional telecom C-band, thus mitigating the fiber nonlinearity issue. However, the significant dispersion slope of NZ-DSF compromises the bandwidth over which good transmission performance can be achieved. Following these considerations, it is relevant to identify the CD-induced operating bandwidth of single-mode optical fibers, which is defined by the effect of power fading in IM-DD optical systems[25] and is indeed dependent on the transmission wavelength. Other solutions for the mitigation of CD effects rely on either the use of complex digital signal processing at the receiver[26] or the manipulation of the signal at the transmitter using means like in-phase-quadrature-phase-modulated complex single-sideband formats (IQ-DD)[27] or Tomlinson–Harashima precoding (THP)[28]-[29], in order to extend the reach. However, the IQ-DD approach significantly increases the expense of both electrical and optical components at the transmitter and also suffers from a high carrier-to-signal power ratio restriction, whilst the THP-based IM-DD scheme exhibits a much higher computational complexity and degraded transmission performance in wavelength-division multiplexing (WDM) transmission and adds additional processing latency. In contrast to the schemes discussed above, HCFs offer a fundamentally different way to realize spectrally flat low dispersion profiles over wide bandwidths whilst maintaining ultra-low nonlinearity. This unique nature of HCFs provides the potential to achieve high-speed wide-band IM-DD transmission in a way that is not possible with conventional solid-core fibers.

In this work, we simultaneously address the challenges of overcoming the latency, nonlinearity and CD issues without increasing system complexity, by using hollow-core NANF as a transmission medium in a high-speed WDM system. We report the first experimental comparison of the transmission performance between a hollow-core NANF, solid-core SSMF and solid-core NZ-DSF, demonstrating the longest transmission experiment comprising solely HCF to date. Using the NANF, we achieve transmission at 200 Gb/s (4×50G) and 400 Gb/s (4×100G) over distances of 142.8 km and 38.1km, respectively. Compared to SSMF and NZ-DSF, the reach improvement is five and two times, respectively, under the same experimental conditions. To the best of our knowledge, this constitutes the longest CD-uncompensated simple IM-DD WDM C-band transmission demonstrations based solely on HCF. By using the hollow-core NANF for >100-km transmission, we achieve a significant >150-μs latency reduction compared to solid-core fibers, resulting in a ~31% improvement.

2. Numerical and Experimental Characterizations of the Hollow-core NANF

2.1. 4.76-km Hollow-core NANF

Two NANFs, fabricated from separate draws and preforms, were directly spliced to produce a single spool of 4.76-km length. The NANF-to-NANF splicing loss was around 0.1 dB. Both NANFs were designed and fabricated for operation in the first antiresonant window to allow for longer yield as well as an ultrawide bandwidth. The lengths of the two NANFs were ~3.4 km (NANF#1) and ~1.4 km (NANF#2), respectively. NANF#1, which represents the longest continuous draw amongst any antiresonant fiber reported to date, had an average core size and membrane thickness of 36.4 μm and 0.55 μm, respectively. The corresponding values of the average core size and membrane thickness of NANF#2 were 34.6 μm and 0.50 μm, respectively. The average losses of the spliced NANFs in the C- and L-bands range from 1.15 to 1.37 dB/km and from 0.85 to 0.9 dB/km, respectively. The NANF was capable of supporting effective single-mode guidance since the differential loss between the fundamental and any high-order mode (HOM) is extremely high (~100 dB/km) by virtue of the NANF guidance mechanism and

design. The high differential modal loss any HOM content generated, e.g. due to mode mismatch/misalignment at a splice point, is rapidly killed off (over ~10 m length scales) during onward signal propagation[15]-[17]. Further characterisation details on the fibers are reported in a previous work[30].

To facilitate the use of the hollow-core NANF in a conventional optical transmission system, the two ends of the spliced NANF assembly were spliced to FC/APC SSMF patch cords, using a mode field adaptor (MFA) in-between to minimize the mode field diameter mismatch and thus the overall loss of the spliced fiber. These multiple arc-fusion splices contributed about 2 dB to the total insertion loss of the spool, which included ~0.1dB loss for the NANF-NANF splice, and ~0.8/0.9dB at each end for NANF-SSMF spliced interconnection. The total loss of the SSMF-connectorized ~5-km NANF ranged between 7 to 8 dB across the S- to L-band[30]. We note that further optimisation could yield small improvements to these spliced interconnection loss values [31]. Furthermore, it has been demonstrated that splicing-free, glue-based fiber-array technology is another viable way to realize HCF-SSMF connection, with the potential to further reduce the inter-connection loss to 0.3 dB, or so[32]. It is also worth noting that further loss reduction of the NANF can realistically be expected by improvements in fabrication to ensure a more symmetric and uniform fiber structure over the fiber draw and by refinements of structural design, e.g. reduction of the azimuthal inter-tube gaps. Indeed, this has been evidenced in a recent report of a 1.7 km long ~0.28 dB/km transmission loss hollow-core NANF[17], indicating a most promising route towards breaking the fundamental loss limit of solid-core silica fiber. (Note that the 0.28-dB/km NANF was only fabricated after completion of the work reported herein and so was not available for use here).

2.2. CD and Bandwidth Comparison

We first investigated the CD performance of the hollow-core NANF. For comparison, we benchmark the fiber performance against that of SSMF and NZ-DSF, as specified in the International Telecommunication Union (ITU) standards (*G.652* and *G.655*). **Figure 1(a)**

shows the CD of the three different fiber types over 1.400 μm to 1.625 μm, wherein the upper and lower bounds of the SSMF and NZ-DSF are as specified in the ITU standards, whilst the two bounds of the NANF curves represent the simulated CD values of NANF#1 and NANF#2. It is seen that the NANF exhibits a significantly lower CD and a much lower CD slope than the SSMF across the wavelength range from 1.400 μm to 1.625 μm. Compared to the NZ-DSF, the NANF also has a lower absolute CD value at most wavelengths.

We adopted the mean values of the CD ranges of the three types of fiber to numerically investigate their 3-dB bandwidth performance from 1.400 μm to 1.625 μm. Here, the 3-dB bandwidth of each fiber refers to the range of frequencies at which the amplitude of the corresponding simulated CD-induced power fading is reduced by 3 dB. **Figure 1(b)** shows comparisons of the 3-dB bandwidth of 5-km and 100-km fibers. The 3-dB bandwidth of the fibers after 5-km transmission is $\sqrt{20}$ times larger than that of after 100-km transmission. Compared to SSMF, the NANF offers more than twice the bandwidth across the investigated wavelength range. After a 100-km length of NANF, its 3-dB bandwidth is around 12.37 GHz, whereas the corresponding 3-dB bandwidth of the SSMF is 4.42 GHz. Furthermore, compared to the NZ-DSF, the NANF also offers a much broader bandwidth across the wavelengths of interest except for a 60-nm range centred at ~1460 nm (around the zero-dispersion window of the NZ-DSF).

We further conducted experimental CD characterisation measurements on selected fiber lengths using a spectral difference interferometry set-up. The principle and details on the characterisation method have been presented in a previous work[33], hence are omitted here. We note that CD characterization over a wider spectral range can be realized by using other characterization methods, such as the Mach–Zehnder interferometer method together with a super-continuum source[34-35]. To facilitate a direct comparison, our experiments were carried out on spools that were available in our labs, and which had as close a physical length to the

NANF under test as possible (4.76 km). These fibers were a ~4.53-km length of SSMF (*Corning SMF-28e*) and a ~4.73-km length of NZ-DSF (*Corning LEAF*). The measurements were conducted in the C-band (1.530-1.565 μm) (limited by the operational bandwidth of a C-band Waveshaper used in the set-up[33]), and the results are shown in Fig. 1(a). It is confirmed that the NANF exhibits the lowest CD amongst the three types of fibers in the C-band, ranging from 2.05 to 2.14 ps/nm/km within the 35 nm of the C-band. The corresponding CD values of the SSMF and NZ-DSF ranged from 16.32 to 18.14 ps/nm/km and from 2.68 to 5.44 ps/nm/km, respectively.

Using the experimentally measured values of CD of the three fibers at 1550 nm (namely 17.36, 4.26 and 2.10 ps/nm/km, for the SSMF, NZ-DSF and NANF, respectively), we numerically simulated their CD-induced power fading profiles, and plotted them for 5 km and 100 km fiber lengths in **Fig. 2(a)** and **2(b)**, respectively. It is seen that after a 5-km length of fiber, nearly no fading is experienced in the NANF across a 50-GHz bandwidth, whilst power fading starts to emerge at frequencies beyond 30 GHz in the NZ-DSF. In contrast, the SSMF experiences severe power fading, including a spectral null within 30 GHz due to its significantly higher CD. When further extending the fiber length to 100 km, one spectral null is seen at ~17 GHz in the case of the NANF, whereas two spectral nulls are experienced at frequencies around 12 GHz and 21 GHz in the NZ-DSF case. As before, the SSMF exhibits the worst tolerance to CD-induced power fading and the usable bandwidth is restricted to within 5 GHz at this length. In a different visualisation, **Figure 2(c)** shows the 3-dB bandwidth versus fiber length. It is seen that the NANF supports a 12.5-GHz 3-dB bandwidth over a distance of 100 km. This is sufficient for 25 GBaud Nyquist-shaped signals, which occupy a bandwidth of around half the symbol rate owing to the Nyquist pulse shaping[36]. Consequently, a data rate of 50 Gb/s can be achieved over a distance of 100 km with the help of Nyquist 4-ary pulse amplitude modulation (PAM4) which has a spectral efficiency of 2 bits/symbol. We note that in practical optical transmission systems, a bandwidth beyond the absolute 3 dB limit is generally exploited to achieve a higher

capacity. In this regard, if we consider the 12-dB bandwidth which is ~1.3 times wider than the 3-dB bandwidth, the maximum transmission reach enabled by the NANF is twice as long as that of the NZ-DSF at this wavelength (~150 km for a 12.5-GHz bandwidth and ~50 km for a 25-GHz bandwidth).

It is to be noted that it is of course possible to design solid-core dispersion-shifted fibers with a low CD slope over a broad bandwidth, which can present a much broader bandwidth than the standardized fibers considered in this work. Indeed, the use of such fibers in WDM transmission has been extensively considered in the past, but it was shown that the impact of fiber nonlinearities, e.g., four-wave mixing can give rise to significant penalties, prohibiting their use even at the length scales considered here[37]. In contrast, the NANF has already been shown to have significantly lower fiber nonlinearity compared to SSMF, which means that transmission in NANF is effectively nonlinearity-free[18].

In addition to CD, nonlinearity and loss, other potential physical effects could compromise transmission performance including multipath interference and polarization mode dispersion/loss, however it is worth noting that data transmision has already been succesfully been reported over longer distances than here (for more sensitive coherent data formats) using the same fiber[22]. Hence, we do not believe that such effects played a limiting role in the experiments reported herein.

3. Transmission Set-up and Results

3.1. Experimental setup

We implemented an IM-DD WDM optical re-circulating loop to investigate the transmission performance of the NANF over a longer reach. By inserting the three similarly long fibers (~5 km) into the loop, one at a time, we were able to perform a comparison of the transmission performance of the NANF relative to that of the more conventional solid-core transmission fibers (SSMF and NZ-DSF). **Figure 3** shows the set-up of the IM-DD re-circulating loop system. The IM transmitter was formed by four 16-dBm tunable lasers (*ID Photonics CoBrite*

DX4) operating at 1549.32 nm, 1550.12 nm, 1550.92 nm and 1551.72 nm which were coupled into a $LiNbO_3$ Mach-Zehnder modulator (MZM) via a 4×1 polarisation maintaining optical coupler. The modulation signals were generated using a 90-GSa/s arbitrary waveform generator (AWG, *Keysight M8196A*). They were electrically amplified and fed to the $LiNbO_3$ MZM. To de-correlate the four WDM channels, a Waveshaper (*Finisar 4000E*) was used to separate the odd and even channels. The two groups of channels were transmitted in dissimilar lengths of optical fiber and then recombined together via a 3-dB optical coupler. The four de-correlated WDM channels, with a total power of around -3.0 dBm, were then fed into a booster EDFA (EDFA1). The amplifier had a typical noise figure of <5 dB and was operated at its maximum output power of 18.5 dBm. A variable optical attenuator (VOA1) was adopted to adjust the input power to the transmitter acousto-optic modulator (AOM1). The output of AOM1 was then directed into the loop via a 50:50 optical coupler. An optical bandpass filter (OBPF1, *Alnair Labs BVF-300CL*) with a bandwidth of 3.2 nm, was included in the loop. Note that OBPF1 has a flat-top passband and a roll-off of 1500 dB/nm on its edges, ensuring an out-of-band suppression of more than 40 dB. A second VOA (VOA2) was used to adjust the launch power into the transmission fiber, as well as to compensate for the loss difference between the three types of fibers, so as to balance the gain and loss of the loop.. As aforementioned, the three lengths of SSMF, NZ-DSF and NANF were tested one by one. After the fiber, an in-loop EDFA (EDFA2, typical noise figure of 4.3 dB) was used for optical amplification. The input power of EDFA2 was fixed to -6.7 dBm in all three fiber cases by adjusting VOA2. In this way, the noise level for the different fiber types was maintained identical to ensure a fair comparison. Whilst operating the amplifier in the constant-gain mode, its output power was maintained at its maximum value of 15 dBm to ensure the same noise contribution in all three fiber cases. Note that although the NANF can tolerate a much higher input optical power[18], EDFA2 was adopted after the fiber to keep the nonlinearity low in the SSMF/NZ-DSF cases and provide for a fairer comparison. The output of EDFA2 was connected to an in-loop AOM (AOM2) whose output

was sent to the second input of the 50:50 optical coupler to close the loop. The rise time of the AOMs is <100 ns and they were controlled by two complementary pulses generated by a pulse generator (*Standard Research Systems DG535*). The loading state (switch-on time of AOM1) and looping state (switch-on time of AOM2) lasted two and fifty loops in the experiments, respectively. The output of the loop was collected by a DD receiver, which included a receiver-side OBPF (OBPF2) to select the WDM channels for performance evaluation, a VOA (VOA3) to adjust the received optical power (ROP) at the photodetector (PD, *Finisar XPRV2022A*) and a 99:1 tap coupler and power meter for ROP monitoring. The ROP at the photodetector was fixed to -7 dBm for all transmission cases shown below; this value offered optimal performance in the PD[30]. The detected signals at the PD were then recorded by an 80-GSa/s digital storage oscilloscope (DSO, *Agilent DSO-X 93204A*) for further offline digital signal processing (DSP). We note that the use of polarisation scrambling in our loop proved unfeasible, because of the relatively high polarisation-dependent loss of OBPF2 at the receiver. Nevertheless, in separate measurements we have ensured that the polarisation-dependent loss of the hollow-core NANF is negligible [19] and we carried out the transmission in this work without any polarisation control in place. It is also worth noting that as indicated in the analysis presented in the previous section, the limiting factor in IM-DD transmission of signals in both the SSMF and NZ-DSF is the CD-induced power fading rather than the fiber loss and the available signal-to-noise ratio (SNR). Even though the lower transmission loss of SSMF/NZ-DSF would allow longer spans to be adopted in these fiber types, we opted instead for similar physical lengths, so that the effect of amplification noise would not be a factor in our comparison. The justification of this choice will become evident in the presentation of our experimental results below.

In this work, we experimented with three different modulation signals in our tests, namely 50-Gb/s/λ Nyquist non-return-to-zero (NRZ) on-off keying (OOK), 50-Gb/s/λ Nyquist PAM4 and 100-Gb/s/λ Nyquist PAM4. In the offline DSP, at the transmitter, the mapped OOK or PAM4 symbols were 90 times up-sampled and then filtered by a square-root-raised-cosine (SRRC)

filter. The roll-off factor and span of the SRRC filter were 0.1 and 20, respectively. To generate the 50-Gb/s OOK/100-Gb/s PAM4 signals or 50-Gb/s PAM4 signals, the filtered signals were 50- or 25-times down-sampled before been fed into an AWG operated at 90 GSa/s. At the receiver, the electrical signals detected at the photodetector were captured by an 80-GSa/s DSO. The recorded data was first synchronized using the correlation-based method, followed by a re-sampling operation. The re-sampled data was then filtered by a matched SRRC filter. Subsequently, the resulting data was equalized by a T/2-spaced decision-feedback equalizer wherein the recursive least-squares algorithm was adopted[19], and the numbers of feedforward and feedback taps of the equalizer were 17 and 7, respectively. Finally, the equalized data was OOK- or PAM4-demapped, and the de-mapped binary bits were used for error counting to obtain the BER of the transmission. The traces of the optical spectra of the WDM channels at the transmitter for these three cases are shown in the **inset in Fig. 3**, and below we will present the results achieved with each one.

3.2. Experimental Results

3.2.1. 4×50-Gb/s OOK WDM Transmission

The bit error rate (BER) results for 4×50-Gb/s OOK WDM transmission are shown in **Fig. 4**, together with electrical spectra and eye diagrams of the 1550.92-nm channel at different reaches and for the different fibers. It is seen in Fig. 4(a) that at the BER threshold of 3.8×10^{-3} for 7% forward error correction (FEC), the achievable transmission distances of the four WDM channels were <22.67 km, ~56.75 km, ~104.69 km in the SSMF, NZ-DSF and NANF, respectively. When considering the 20% FEC BER limit of 2×10^{-2}, the corresponding reaches were ~31.74 km, ~75.67 km, and ~142.76 km, respectively. In both FEC limit cases, the NANF offered ~2 times and ~5 times the reach compared to the NZ-DSF and SSMF, respectively. Figure 4(b)-4(d) show the corresponding electrical spectra and eye diagrams around the 20% FEC limit in the three fiber cases, together with the recorded BER and number of circulations for each respective case. In the SSMF case, three spectral nulls occurred after 31.74-km

transmission, and their specific frequencies were around 10.6 GHz, 18.4 GHz, and 23.8 GHz. We note that the analytical expression for the frequencies of the spectral nulls is $f_{null} = \sqrt{Nc/(2D\lambda^2 L)}$, $N = 1,3,5,\ldots$, where c is the light speed, D is the value of CD at wavelength λ, and L is the transmission distance. In comparison, two spectral nulls (~13.9 GHz and 24.1 GHz) were experienced in the NZ-DSF case after 75.67-km transmission. It is evident that the NANF suffered from a less significant power fading effect due to its low CD (two spectral nulls occurred at ~14.4 GHz and 25.0 GHz), even though the transmission distance in the NANF (i.e., 142.76 km) was so much longer than in the other two fiber types for the cases considered in the figure. Furthermore, it is seen in Fig. 4 that under the 20% FEC limit, the transmission distance limit was reached where the first frequency null occurred at ~10.5 GHz in the SSMF case, whereas this value was around 14.5 GHz in the NANF case. This resulted from the more pronounced accumulated amplified spontaneous emission (ASE) noise from the in-loop EDFA, since many more loops were experienced in the NANF case. Therefore, unlike the SSMF case, the ASE noise was also a potential limiting factor to transmission performance in the NANF case, although the CD should still be the dominant factor as a severe spectral null was experienced within the signal's bandwidth. This view is supported by the numerically simulated profiles of the CD-induced power fading in Fig. 4 which align well with the experimental measurements.

3.2.2. 4×50-Gb/s and 4×100-Gb/s PAM4 WDM Transmission

We next transmitted Nyquist PAM4 signals at 50 Gb/s/λ and 100 Gb/s/λ in the re-circulating loop. The corresponding results are shown in **Fig. 5**. In the 4×50-Gb/s case, taking the 20% FEC BER limit as an example, the achievable distances in the SSMF and NZ-DSF were around 20 km and 70 km, respectively. By using the NANF instead, the reach was further extended to ~120 km. Compared to the 4×50-Gb/s OOK transmission, it is seen that the respective achievable reaches using the three fibers at the two BER thresholds were shorter for the 4×50-

Gb/s PAM4 transmission. This is because the PAM4 format, while occupying half the signal bandwidth, inherently requires a much higher SNR to achieve a comparable BER to that of the OOK format. However, the accumulated noise from the in-loop EDFA in the short-span re-circulating loops will continuously degrade the SNR of the system. This explains the shorter reaches compared to that of the 4×50-Gb/s OOK transmission, and also indicates that it was the accumulated amplifier noise rather than the CD that dominated the transmission performance in the 4×50-Gb/s PAM4 transmission.

In the 4×100-Gb/s case (Figure 5(b)), the BER of the signal transmitted in the SSMF was far above the 20% FEC limit even after a transmission distance of ~9 km, due to a severe spectral null occurring within the signal's bandwidth (at ~20 GHz). By using the NZ-DSF and NANF, reaches of ~19 km and ~38 km were achieved with BERs around the 20% FEC limit, respectively. In the NANF, BERs below the 7% FEC limit for all four WDM channels were possible after a transmission distance of ~25 km, whereas the maximum reach at the 20% FEC limit is ~38 km.

3.2.3. Comparison of Transmission Latency

Apart from the low CD in a low nonlinearity medium, transmission in the NANF also benefits from ultimate low-latency propagation, as compared to any other types of solid-core fiber, including SSMF and NZ-DSF. We have experimentally measured the latencies in ~4.53-km SSMF, ~4.73-km NZ-DSF and ~4.76-km NANF by partially filling the re-circulating loop and measuring the interval between adjacent discontinuities in the time-domain waveforms. The measured intervals for the three fiber lengths were measured as 22.47 μs, 23.42 μs and 16.28 μs, respectively, corresponding to 4.96 μs/km, 4.95 μs/km, and 3.42 μs/km, respectively. Therefore, the corresponding effective refractive indices of the three fibres were around 1.487, 1.484, and 1.025, respectively. Based on these measured values, a comparison of the transmission latency within a single-span (~5 km) and up to 50 loops (~250 km) is depicted in **Fig. 6**. It is seen that the transmission latencies of the SSMF and NZ-DSF are nearly identical

as the group velocity in these two fiber types were comparable. In contrast, due to its air-guided property, the hollow-core NANF exhibits a much lower transmission latency. As shown in Fig. 6 (a), for a single spool transmission of ~ 5-km length, the reduction in latency was more than 7 μs. When further extending the transmission reach via the re-circulating loop, the latency reductions brought by using the hollow-core NANF instead of the solid-core fiber were more than 150 μs and around 310 μs for 100-km and 200-km cases, respectively, as shown in Fig. 6(b). The corresponding measured latency performance improvements of the hollow-core NANF were ~31.05% and ~30.91% compared to the SSMF and NZ-DSF, respectively.

4. Discussion and Conclusion

We report the longest IM-DD WDM transmission based solely on HCF, which simultaneously tackles the challenges of CD-induced power fading and fiber latency in longer-haul applications. Our demonstration suggests a fundamentally different route to realising high-speed simple IM-DD long-reach WDM fiber transmission at ultimate low-latency. We have validated this by experimentally comparing the transmission performance in a hollow-core NANF against that in SSMF and NZ-DSF. These proof-of-concept experiments were carried out in the C-band using an optical re-circulating loop, showing that reach improvements of ~5 and ~2 times can be achieved in the NANF relative to using the SSMF and NZ-DSF, respectively. 4×50-Gb/s and 4×100-Gb/s IM-DD transmissions were demonstrated at transmission distances of about 143 km and 38 km, respectively. Moreover, it was validated that the HCF-based transmission can offer ~31% latency reduction compared to both SSMF and NZ-DSF, saving more than 150-μs transmission time when the link distance is beyond 100 km.

Due to the availability of limited lengths of NANF samples for our transmission experiments, we resorted to using a re-circulating loop with a short fiber span in our tests. While this proved to be a powerful experimental tool, allowing us to finely resolve the performance degradation over fiber length for the three fiber types we considered, extra gain is needed to compensate for the loss of the loop switches (i.e., the two AOMs) and the 50:50 optical coupler. Therefore, it

is anticipated that better transmission performance could be achieved in a straight-line system configuration once longer lengths of NANF become available. In this context, the presented transmission experiments masked the question of fiber loss, which with the current sample, stands greater in NANF than in standard transmission fibers. In order to cover the transmission distances we considered at the loss level of the NANF used here, a much larger number of optical amplifiers would need to be employed in the link relative to the case of a solid-core fiber, which would likely prove to be both impractical and costly. However, recent works have suggested that by refining the structure of the hollow-core NANF as well as improving the fabrication process, the loss gap between NANF and the solid-core SSMF/NZ-DSF can be significantly narrowed[17], indeed to the extent that transmission over the distances explored in this work could be achieved in a single amplification span. Ultimately, it is predicted that the hollow-core NANF has the potential to break the fundamental loss limit of silica solid-core fibers, while satisfying the requirements for ultimate low-latency, ultra-low nonlinearity and CD at the same time[9].

The HCF properties of low dispersion and low dispersion slope over an extremely wide bandwidth enable simplified dispersion management in WDM transmission, in a manner that has not been possible in dispersion engineered solid-core silica fibers, where the impact of fiber nonlinearity has proven prohibitive. While the current experimental validations have been performed in the C-band due to the unavailability of optical components to construct a re-circulating loop set-up (e.g., suitably wideband optical amplifiers, filters and acousto-optic modulators), we anticipate that wide-band IM-DD transmission is realistically achievable in HCFs as assured by their broadband nature. The results we have presented here, in combination with recent reports demonstrating the fabrication of HCFs with losses of 0.28 dB/km[17], indicate that such fibers present a promising route to the realisation of simple, cost-effective, high-capacity, ultra-low-latency IM-DD WDM transmission links with the potential to enable the sustainable growth of latency-critical computer network applications by increasing the

flexibility in the geographical distribution of edge cloud infrastructure, and ultimately, to revolutionize the implementation of optical transmission systems in the years to come.

Acknowledgements

This work was supported by the UK's EPSRC under the Airguide Photonics Programme Grant (EP/P030181/1), the COALESCE project (EP/P003990/1), as well as through the ERC Lightpipe project (682724). Y. Hong acknowledges S.H. Wu from University of Southampton for his help with the Table of Contents graphic.

Conflict of Interest

The authors declare no conflict of interest.

Data Availability Statement

The data for this work is accessible through the University of Southampton Institutional Research Repository (DOI: https://doi.org/10.5258/SOTON/D1864).

Received: ((will be filled in by the editorial staff))
Revised: ((will be filled in by the editorial staff))
Published online: ((will be filled in by the editorial staff))

References

[1] E. Agrell, M. Karlsson, A. R. Chraplyvy, D. J. Richardson, P. M. Krummrich, P. Winzer, K. Roberts, J. K. Fischer, S. J. Savory, B. J. Eggleton, M. Secondini, F. R. Kschischang, A. Lord, J. Prat, I. Tomkos, J. E. Bowers, S. Srinivasan, M. Brandt-Pearce, and N. Gisin, J. Opt. **18**, 063002 (2016).

[2] D. J. Richardson, Science **330**, 327–328 (2010).

[3] X. Liu, and F. Effenberger, J. Opt. Commun. Netw. **8**, B70-B79 (2016).

[4] B. Teipen, M. Filer, H. Grießer, M. Eiselt, and J. P. Elbers, in: Proceedings of European Conference on Optical Communication (ECOC), Amsterdam, Netherlands, 2012, paper P4.07.

[5] V. Bobrovs, S. Spolitis, G. Ivanovs, in: Proceedings of SPIE **9008**, Optical Metro Networks and Short-Haul Systems VI, San Francisco, USA, 2014, paper 90080C.

[6] R. Nagarajan, M. Filer, Y. Fu, M. Kato, T. Rope, and J. Stewart, J. Opt. Commun. Netw. **10**, B25-B36 (2018).

[7] Y. Sagae, T. Matsui, K. Tsujikawa, and K. Nakajima, J. Light. Technol. **37**, 5028-5033 (2019).

[8] F. Poletti, N. V. Wheeler, M. N. Petrovich, N. Baddela, E. N. Fokoua, J. R. Hayes, D. R. Gray, Z. Li, R. Slavik, and D. J. Richardson, Nat. Photon. **7**, 279–284 (2013).

[9] F. Poletti, Opt. Express **22**, 23807-23828 (2014).

[10] S. Gao, Y. Wang, W. Ding, D. Jiang, S. Gu, X. Zhang, and P. Wang, Nat Commun. **9**, 2828 (2018).

[11] P. P. Mitra, and J. B. Stark, Nature **411**, 1027–1030 (2001).

[12] R. J. Essiambre, G. J. Foschini, G. Kramer, and P. J. Winzer, Phys. Rev. Lett. **101**, 163901 (2008).

[13] A. D. Ellis, J. Zhao, and D. Cotter, J. Light. Technol. **28**, 423-433 (2010).

[14] D. J. Richardson, N. V. Wheeler, Y. Chen, J. R. Hayes, S. R. Sandoghchi, G. T. Jasion, T. D. Bradley, E. N. Fokoua, Z. Liu, R. Slavik, P. E. Horak, M. N. Petrovich, and F. Poletti, in: Proceedings of Optical Fiber Communication Conference (OFC), Los Angeles, USA, 2017, paper Tu3H.1.

[15] H. Sakr, Y. Hong, T. D. Bradley, G. T. Jasion, J. R. Hayes, H. Kim, I. A. Davidson, E. N. Fokoua, Y. Chen, K. R. H. Bottrill, N. Taengnoi, N. V. Wheeler, P. Petropoulos, D. J. Richardson, and F. Poletti, J. Light. Technol. **38**, 159-165 (2020).

[16] T. D. Bradley, G. T. Jasion, J. R. Hayes, Y. Chen, L. Hooper, H. Sakr, M. Alonso, A. Taranta, A. Saljoghei, H. C. Mulvad, M. Fake, I. A. K. Davidson, N. V. Wheeler, E. N. Fokoua, W. Wang, S. R. Sandoghchi, D. J. Richardson, and F. Poletti, in: Proceedings of European Conference on Optical Communications (ECOC), Dublin, Ireland, 2019, postdeadline paper PD3.1.

[17] G. T. Jasion, T. D. Bradley, K. Harrington, H. Sakr, Y. Chen, E. N. Fokoua, I. A. Davidson, A. Taranta, J. R. Hayes, D. J. Richardson, and F. Poletti, in: Proceedings of Optical Fiber Communication Conference (OFC), San Diego, USA, 2020, postdeadline paper Th4B.4.

[18] Z. Liu, B. Karanov, L. Galdino, J. R. Hayes, D. Lavery, K. Clark, K. Shi, D. J. Elson, B. C. Thomsen, M. N. Petrovich, D. J. Richardson, F. Poletti, R. Slavik, and P. Bayvel, J. Light. Technol. **37**, 909-916 (2019).

[19] Y. Hong, H. Sakr, N. Taengnoi, K. R. H. Bottrill, T. D. Bradley, J. R. Hayes, G. T. Jasion, H. Kim, N. K. Thipparapu, Y. Wang, A. A. Umnikov, J. K. Sahu, F. Poletti, P. Petropoulos, and D. J. Richardson, J. Light. Technol. **38**, 2849-2857 (2020).

[20] V. A. J. M. Sleiffer, Y. Jung, N. K. Baddela, J. Surof, M. Kuschnerov, V. Veljanovski, J. R. Hayes, N. V. Wheeler, E. R. N. Fokoua, J. P. Wooler, D. R. Gray, N. H. L. Wong, F. R. Parmigiani, S. Alam, M. N. Petrovich, F. Poletti, D. J. Richardson, and H. Waardt, J. Light. Technol. **32**, 854-863 (2014).

[21] M. Kuschnerov, V. A. J. M. Sleiffer, Y. Chen, E. Man, Y. Chen, Z. Liu, S. R. Sandoghchi, G. T. Jasion, T. D. Bradley, E. N. Fokoua, J. R. Hayes, N. V. Wheeler, D. R. Gray, R. Slavik, Y. Jung, N. L. Wong, B. J. Mangan, F. Poletti, M. N. Petrovich, and D. J. Richardson, in: Proceedings of European Conference on Optical Communications (ECOC), Valencia, Spain, 2015, paper paper Th.1.2.4.

[22] A. Nespola, S. Straullu, T. D. Bradley, H. C. Mulvad, J. R. Hayes, G. T. Jasion, M. A. Gouveia, S. R. Sandoghchi, S. Bawn, F. Forghieri, D. J. Richardson, F. Poletti, and P. Poggiolini, in: Proceedings of European Conference on Optical Communications (ECOC), Dublin, Ireland, 2019, postdeadline paper PD1.5.

[23] K. Zhong, X. Zhou, J. Huo, C. Yu, C. Lu, and A. P. T. Lau, J. Light. Technol. **36**, 377-400 (2018).

[24] B. Karanov, D. Lavery, P. Bayvel, and L. Schmalen, Opt. Express **27**, 19650-19663 (2019).

[25] A. Yekani, and L. A. Rusch, IEEE Trans. Commun. **67**, 2908-2913 (2019).

[26] X. Tang, S. Liu, Z. Sun, H. Cui, X. Xu, J. Qi, M. Guo, Y. Lu, and Y. Qiao, Opt. Express **27**, 25708-25717 (2019).

[27] A. Mecozzi, C. Antonelli, and M. Shtaif, Optica **3**, 1220-1227 (2016).

[28] K. Matsumoto, Y. Yoshida, A. Maruta, A. Kanno, N. Yamamoto, and K. Kitayama, in: Proceedings of Optical Fiber Communication Conference (OFC), Los Angeles, USA, 2017, paper Th3D.7.

[29] Q. Hu, K. Schuh, M. Chagnon, F. Buchali, S. T. Le, and H. Bülow, in: Proceedings of European Conference on Optical Communications (ECOC), Rome, Italy, 2018, paper We3F.6.

[30] Y. Hong, T. D. Bradley, N. Taengnoi, K. R. H. Bottrill, J. R. Hayes, G. T. Jasion, H. C. Mulvad, F. Poletti, P. Petropoulos, and David J. Richardson, in: Proceedings of Optical Fiber Communication Conference (OFC), San Diego, USA, 2020, paper W3E.3.

[31] T. D. Bradley, J. R. Hayes, Y. Chen, G. T. Jasion, S. R. Sandoghchi, R. Slavík, E. N. Fokoua, S. Bawn, H. Sakr, I. A. K. Davidson, A. Taranta, J. P. Thomas, M. N. Petrovich, D. J. Richardson, and F. Poletti, in: Proceedings of European Conference on Optical Communications (ECOC), Rome, Italy, 2018, postdeadline paper Th3F.2.

[32] M. Komanec, D. Suslov, S. Zvánovec, Y. Chen, T. Bradley, S. R. Sandoghchi, E. R. Numkam Fokoua, G. T. Jasion, M. N. Petrovich, F. Poletti, D. J. Richardson, and R. Slavík, IEEE Photon. Technol. Lett. **31**, 723-726 (2019).

[33] K. R. H. Bottrill, M. A. Ettabib, I. Demirtzioglou, R. Marchetti, C. Lacava, F. Parmigiani, D. J. Richardson, and P. Petropoulos, Laser Photonics Rev. **13**, 1900007 (2019).

[34] X. Wang, D. Ge, W. Ding, Y. Wang, S. Gao, X. Zhang, Y. Sun, J. Li, Z. Chen, and P. Wang, Opt. Lett. **44**, 2145-2148 (2019).

[35] G. M. Ponzo, M. N. Petrovich, X. Feng, P. Horak, F. Poletti, P. Petropoulos, and D. J. Richardson, Opt. Express **22**, 943-953 (2014).

[36] N. Kikuchi, and R. Hirai, in: Proceedings of European Conference on Optical Communications (ECOC), Cannes, France, 2014, paper P.4.12.

[37] R. W. Tkach, A. R. Chraplyvy, F. Forghieri, A. H. Gnauck, R. M. Derosier, J. Light. Technol. **13**, 841-849 (1995).

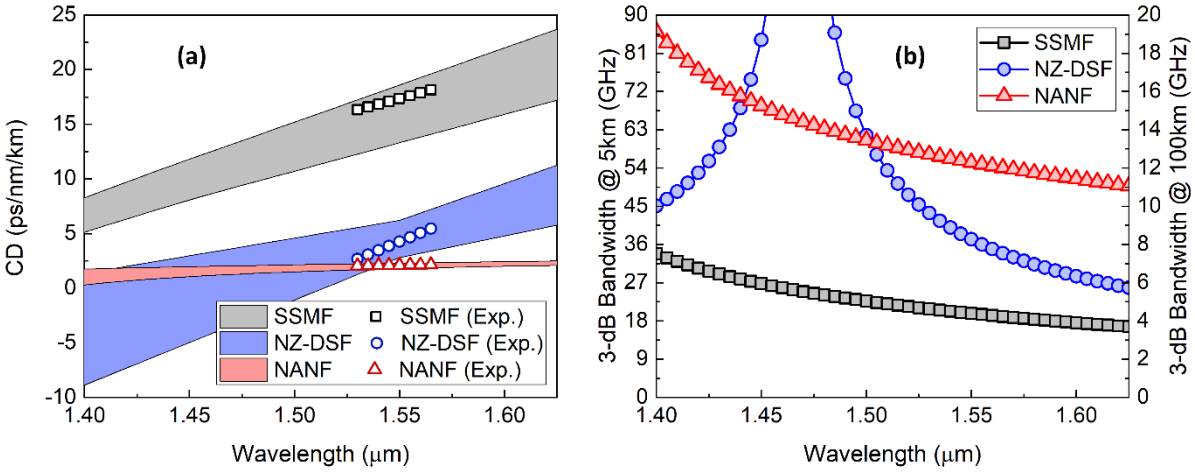

Figure 1. Comparisons of CD and bandwidth amongst SSMF, NZ-DSF and NANF for 1.400-1.625 μm. (a) CD values versus wavelength (the symbols show experimentally measured values); and (b) numerically calculated fibers' 3-dB bandwidths versus wavelength over a length of 5 km and 100 km.

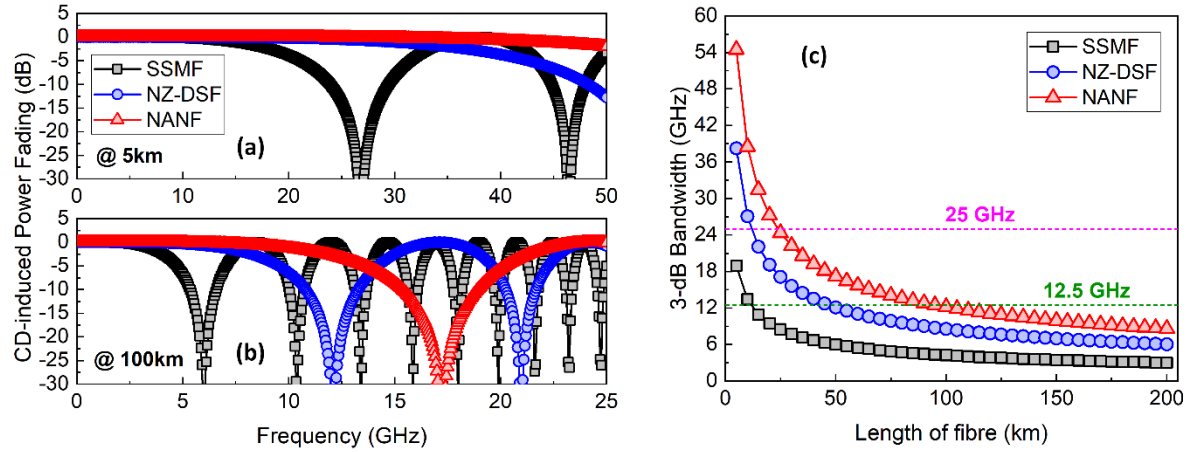

Figure 2. Comparisons of CD-induced power fading versus frequency and fiber bandwidth versus reach amongst SSMF, NZ-DSF and NANF at 1550 nm. CD-induced power fading over frequencies after a length of (a) 5 km and (b) 100 km, and (c) fiber 3-dB bandwidth versus length of fiber.

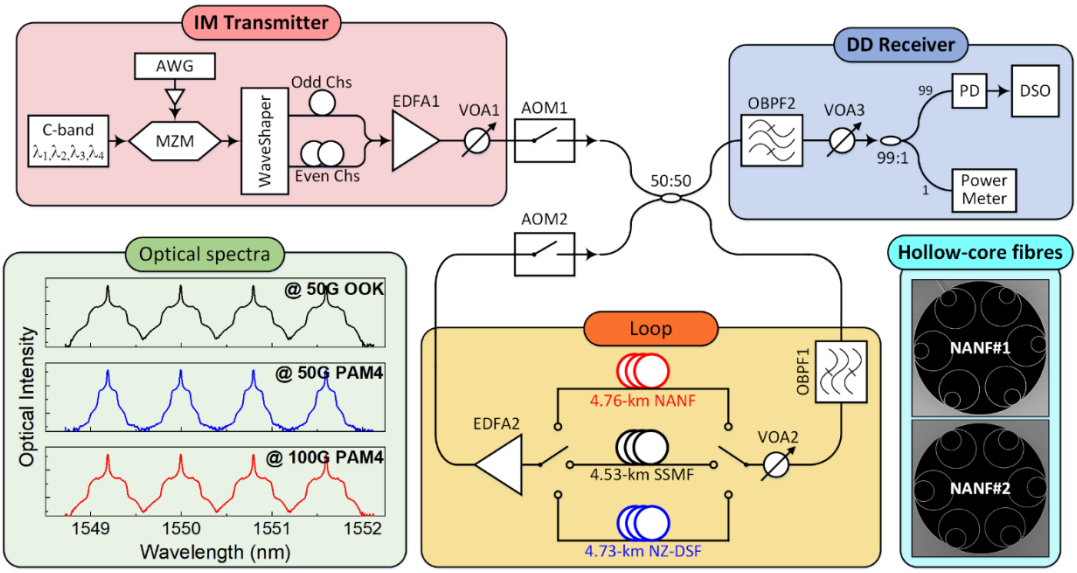

Figure 3. Experimental set-up of the IM-DD WDM optical re-circulating loop. Inset (left): optical spectra of the WDM channels at the transmitter using 50-Gb/s/λ Nyquist OOK, 50-Gb/s/λ Nyquist PAM4, and 100-Gb/s/λ Nyquist PAM4. Inset (right): the cross-sectional scanning electron microscope (SEM) images of the two hollow-core NANFs, showing their relatively symmetric fiber cross-sections.

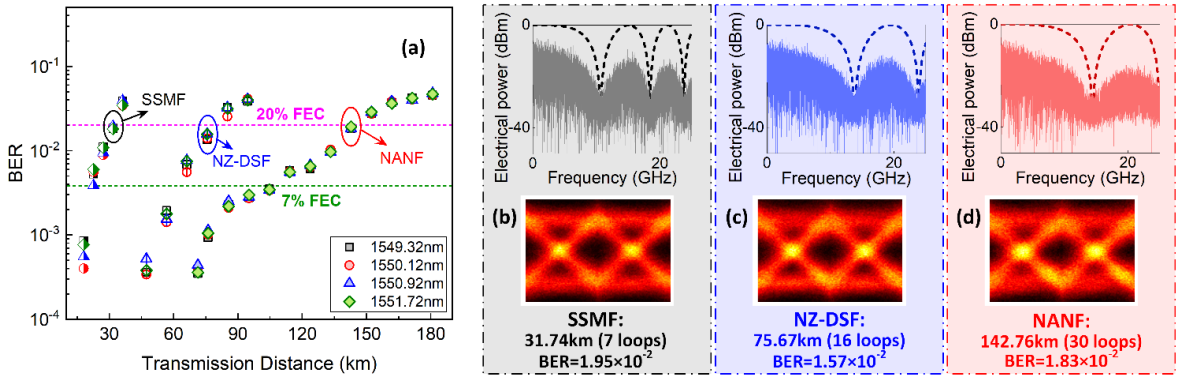

Figure 4. (a) BER versus distance of 4×50-Gb/s OOK WDM transmission, and electrical spectrum and eye diagram of the 1550.92-nm channel after (b) 31.74-km length of SSMF, (c) 75.67-km length of NZ-DSF, and (d) 142.76-km length of NANF. The dash lines shown in Fig. 4(b)-4(d) represent the simulated CD-induced power fading profiles under the same reach, and the corresponding numbers of loops and BERs are also shown in Fig. 4(b)-4(d).

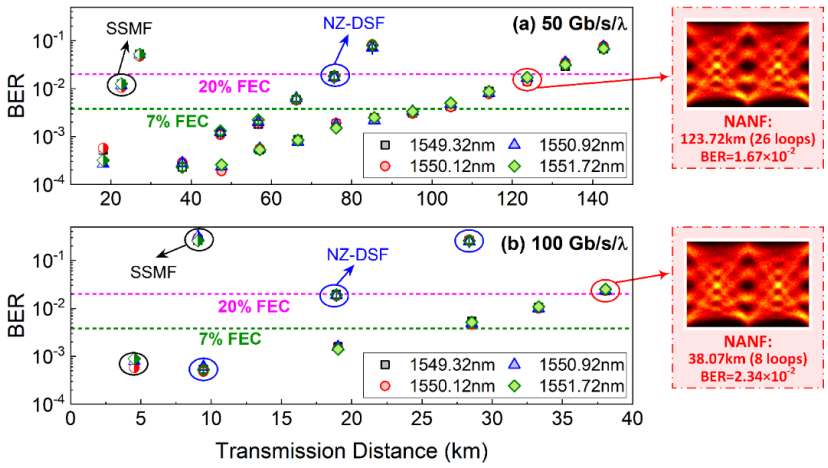

Figure 5. (a) BER versus distance of 4×50-Gb/s PAM4 WDM transmission, and (b) BER versus distance of 4×100-Gb/s PAM4 WDM transmission. Insets: eye diagrams and the corresponding BERs of the 1550.92-nm channel after 123.72-km length of NANF and 38.07-km length of NANF in the 4×50G and 4×100G cases, respectively.

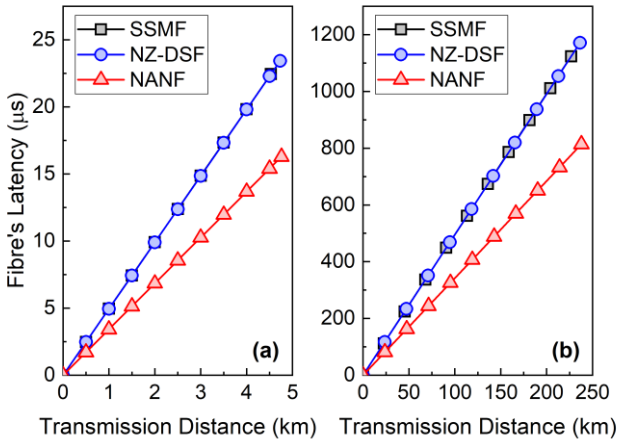

Figure 6. Comparisons of latency in propagation amongst the SSMF, NZ-DSF and NANF. (a) within a single-loop transmission and (b) up to 50-loop transmission.